*Ecological Applications*, 26(7), 2016, pp. 2225–2237


# Landscape-scale consequences of differential tree mortality from catastrophic wind disturbance in the Amazon

Sami W. Rifai,[1,9] José D. Urquiza Muñoz,[2] Robinson I. Negrón-Juárez,[3] Fredy R. Ramírez Arévalo,[2] Rodil Tello-Espinoza,[2] Mark C. Vanderwel,[4] Jeremy W. Lichstein,[5] Jeffrey Q. Chambers,[3,6,7] and Stephanie A. Bohlman[1,8]

[1]*School of Forest Resources and Conservation, University of Florida, Gainesville, Florida 32611 USA*
[2]*Facultad de Ciencias Forestales, Universidad Nacional Amazonía Peruana, Iquitos, Perú*
[3]*Climate Sciences Department, Earth Sciences Division, Lawrence Berkeley National Laboratory, Berkeley, California 94720 USA*
[4]*Department of Biology, University of Regina, 3737 Wascana Pkwy, Regina, SK, S4S 0A2, Canada*
[5]*Department of Biology, University of Florida, Gainesville, Florida 32611 USA*
[6]*Department of Geography, University of California, Berkeley, California 94720 USA*
[7]*Instituto Nacional de Pesquisas da Amazônia, Coordenação de Pesquisas de Silvicultura Tropical, 69060-001, Manaus, Amazonas, Brazil*
[8]*Smithsonian Tropical Research Institute, Apartado 0843–03092, Balboa, Ancon, Republic of Panama*

*Abstract.* Wind disturbance can create large forest blowdowns, which greatly reduces live biomass and adds uncertainty to the strength of the Amazon carbon sink. Observational studies from within the central Amazon have quantified blowdown size and estimated total mortality but have not determined which trees are most likely to die from a catastrophic wind disturbance. Also, the impact of spatial dependence upon tree mortality from wind disturbance has seldom been quantified, which is important because wind disturbance often kills clusters of trees due to large treefalls killing surrounding neighbors. We examine (1) the causes of differential mortality between adult trees from a 300-ha blowdown event in the Peruvian region of the northwestern Amazon, (2) how accounting for spatial dependence affects mortality predictions, and (3) how incorporating both differential mortality and spatial dependence affect the landscape level estimation of necromass produced from the blowdown. Standard regression and spatial regression models were used to estimate how stem diameter, wood density, elevation, and a satellite-derived disturbance metric influenced the probability of tree death from the blowdown event. The model parameters regarding tree characteristics, topography, and spatial autocorrelation of the field data were then used to determine the consequences of non-random mortality for landscape production of necromass through a simulation model. Tree mortality was highly non-random within the blowdown, where tree mortality rates were highest for trees that were large, had low wood density, and were located at high elevation. Of the differential mortality models, the non-spatial models overpredicted necromass, whereas the spatial model slightly underpredicted necromass. When parameterized from the same field data, the spatial regression model with differential mortality estimated only 7.5% more dead trees across the entire blowdown than the random mortality model, yet it estimated 51% greater necromass. We suggest that predictions of forest carbon loss from wind disturbance are sensitive to not only the underlying spatial dependence of observations, but also the biological differences between individuals that promote differential levels of mortality.

*Key words: Amazon; blowdown; canopy gap; downburst; INLA; Iquitos; Loreto; necromass; selective mortality; spectral mixture analysis; tree mortality; wind disturbance; windthrow; wood density.*

## Introduction

The magnitude of tree mortality occurring in a tropical forest can determine its community dynamics, where periods of low mortality (background) promote gap phase replacement and a disturbance event resulting in high mortality can trigger a reset of the community followed by colonization of pioneer species. Much of the published research on tropical tree mortality has focused on background mortality, which is pragmatic considering that tropical forest plot networks, a main source of forest dynamics data, are not well suited to sample spatially aggregated disturbances (Fisher et al. 2008, Chambers et al. 2013). Catastrophic wind disturbances (i.e., events with greater than 5% mortality as defined by Lugo and Scatena 1996) in tropical forests have largely focused on hurricane-prone areas (Brokaw and Grear 1991, Lugo and Scatena 1996, Curran et al. 2008). However, the role of non-hurricane catastrophic wind

Manuscript received 10 September 2015; revised 22 January 2016; accepted 14 March 2016. Corresponding Editor: Y. Pan.
[9]E-mail: srifai@gmail.com

disturbance within tropical forests is increasingly recognized to alter both species composition (Chambers et al. 2009*b*, Marra et al. 2014) and create sudden losses of live biomass (Negrón-Juárez et al. 2010), which will decompose and be returned to the atmosphere as carbon emissions. In the Amazon basin in particular, wind storms can create blowdowns with spatial extents in excess of 30 $km^2$ (Nelson et al. 1994). Amazonian blowdowns are thought to emanate from two meteorological mechanisms: downbursts from convective systems and squall line storms (Garstang et al. 1998). A recent display of the widespread mass mortality induced by a squall line storm was seen in 2005, where approximately 500 million trees were estimated to have died (Negrón-Juárez et al. 2010). Yet not all trees die within a Neotropical blowdown, and the identities of which trees are killed has remained an open question until now. The individual variation in biomass of adult trees can span orders of magnitude, so understanding which trees die is of especial importance for reducing the large uncertainties regarding disturbance and its role in the Amazon's large contribution to global land–atmosphere carbon exchange (Davidson et al. 2012).

Previous research to quantify tropical forest blowdowns has mostly focused on identifying the shape of size frequency distributions of blowdowns (Fisher et al. 2008, Chambers et al. 2009*a*, 2013, Kellner and Asner 2009, Asner 2013). However, no studies to date have quantified how mortality rates vary between trees within tropical forest blowdowns and how this differential mortality will affect estimates of landscape-scale carbon losses. On the contrary, because this was unknown, previous efforts to estimate mortality and necromass from wind disturbance events have had to model mortality as a random uniform process (e.g., Negrón-Juárez et al. 2010). Accurately quantifying the effects of episodic wind disturbances on community and ecosystem dynamics requires information not only on the size–frequency distribution of blowdowns, but also on tree mortality rates within blowdowns in relation to the properties of individual trees (e.g., their size and functional traits, such as wood density) and the physical environment (e.g., topographic position). A key concern related to differential mortality (i.e., non-random or selective mortality) is that large trees contain disproportionate amounts of forest biomass (Clark and Clark 1996). Therefore, if large trees suffer disproportionately high mortality during blowdowns, ignoring differential mortality will lead to underestimation of carbon lost to the atmosphere from the disturbance.

There are several reasons to expect differential tree mortality (i.e., dependence of mortality probability on microsite or individual tree properties) in large blowdowns in the tropics. First, background (non-catastrophic) tree mortality rates in tropical forests depend on the characteristics of individual trees, such as high wood density (Chao et al. 2009, Kraft et al. 2010) and, less consistently, large size (Clark and Clark 1996, Laurance et al. 2000, Thomas et al. 2013). Second, fire, drought, and hurricanes have all been shown to cause differential mortality (Barlow et al. 2003, Nepstad et al. 2007, Curran et al. 2008). Third, studies of wind disturbance in temperate forests have found that increasing tree size (Rich et al. 2007), low wood density (Canham et al. 2001, Rich et al. 2007), and higher topographic position (Sinton et al. 2000) promote probability of death. Finally, tree mortality from wind disturbance has a high potential for spatial autocorrelation because the probability of a tree dying is not independent from its neighbor's fate. A large windthrown tree may directly kill or damage neighbors as it falls, or indirectly affects the probability of neighboring tree mortality due to increased wind exposure. Consequently, accurately predicting landscape mortality will likely require accounting for spatial autocorrelation.

In this study, we consider three questions: (1) How much do landscape and tree structural characteristics predispose a tree to die in an Amazon blowdown? (2) Does quantifying spatial autocorrelation alter the estimated degree of differential mortality? (3) How does incorporation of individual tree-based differential mortality and spatial autocorrelation alter necromass estimation across a forest blowdown landscape?

## Methods

### *Study site*

Using 30-m spatial resolution Landsat Thematic Mapper imagery, we located a blowdown that occurred in late 2009 in the Peruvian Amazon (4.389° S, 73.602° W), roughly 100 km south of Iquitos in the department of Loreto. The vegetation is terra firme forest and receives approximately 3,100 mm rainfall per year (Sombroek 2001). In this study area, elevation ranged from 130 to 160 m, where higher elevation strongly corresponds to hilltop topographic positions, intermediate elevations correspond to slopes and lesser ridgelines, and the lower elevations correspond with depressions and valleys.

### *Blowdown identification and satellite image analyses*

Landsat 5 Thematic Mapper (TM) acquisitions with scene identifiers "LT50060632009245CUB00" (2 September 2008) and "LT50060632009341CUB00" (7 December 2009) were used to assess the pre- and post-disturbance landscape, respectively. The images were atmospherically corrected using the ENVI fast line-of-sight atmospheric analysis of hypercubes (FLAASH; Exelis Visual Information Solutions, Boulder, Colorado, USA) prior to analysis. Chambers et al. (2007) demonstrated that forest wind disturbance can be detected and quantified from Landsat images due to a significant increase in dead woody material or non-photosynthetic vegetation (NPV) in the images, and the change in NPV can be used as a metric of disturbance intensity. Multiple endmember spectral mixture analysis (MESMA; Roberts et al. 1998), a variant of linear spectral

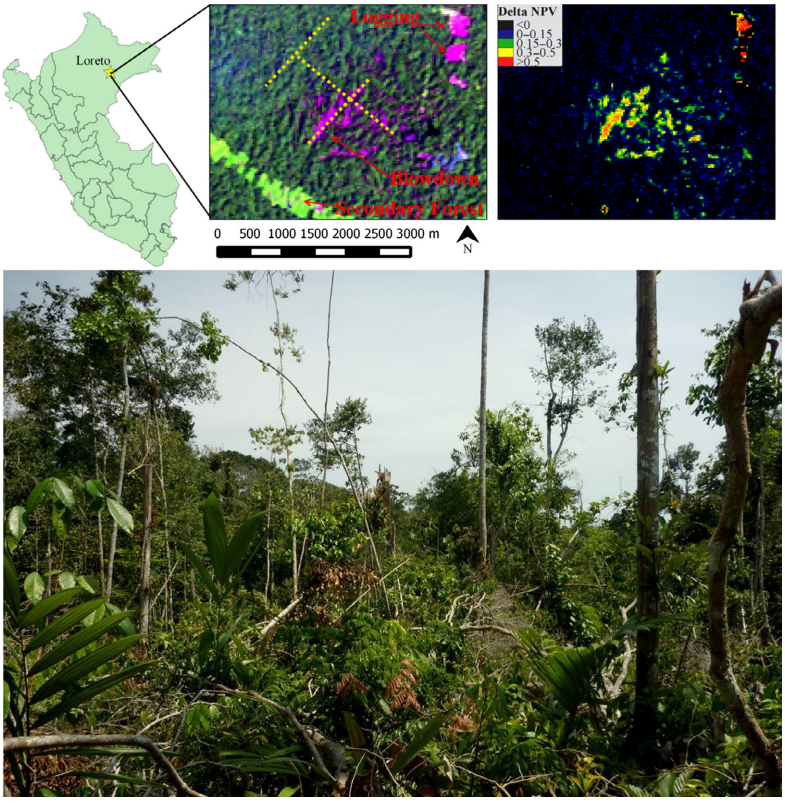


FIG. 1. 2009 blowdown study location roughly 100 km south of Iquitos, Perú in the department of Loreto. The top middle panel shows the post-disturbance Landsat 5 TM (RGB:Bands 5,4,3) with yellow dotted line indicating the position of transect plots. The top right panel shows the variation in disturbance intensity indicated by different categories of ΔNPV (increase in exposed wood detected by pre- and post-disturbance Landsat images). The bottom panel shows a photo from near the center of the blowdown, taken <1 yr after the disturbance event.

unmixing, was used to estimate the pre- and post-disturbance NPV fraction of the blowdown landscape. For the unmixing, we used three endmembers: NPV, green vegetation (GV), and shade. Soil, which is often used as a fourth endmember in forested landscapes, was not used as an endmember because while blowdown events produce a high fraction of windthrown trees, relatively little soil is visible from above. Constrained reference endmember selection (Roberts et al. 1998) was used to derive spectral libraries of the target endmembers from the post-disturbance images. Shade normalization was applied to produce an image of just the fraction of NPV, and the fraction of GV for each pixel. The pre-disturbance fraction of NPV was then subtracted from the post-disturbance fraction of NPV to yield the change in NPV, ΔNPV, image (Chambers et al. 2007, Negrón-Juárez et al. 2010, 2011, Marra et al. 2014). A very similar implementation of the ΔNPV method has been demonstrated to be sensitive to subpixel-scale clustered treefalls composed of as few as six trees (Negrón-Juárez et al. 2011).

To generate landscape topographic variables, we downscaled the AST14DEM digital elevation model (DEM) (*data available online*) from 30- to 10-m spatial resolution through cubic-convolution.[10] Elevation and ΔNPV values were extracted for plot units from the 3-ha transect and the ΔNPV calibration plots (see *Methods: Blowdown identification and satellite image analyses*). Image analysis was performed with ENVI and the VIPER Tools ENVI plugin (*available online*).[11]

### *Field data collection*

Three intersecting transects, consisting of 103 30 × 10 m contiguous plots (3.1-ha total area), were installed inside and outside the blowdown affected area (Fig. 1; hereafter called "transect data"). Disturbed and non-disturbed plots were chosen to have comparable topographic characteristics. Elevation ranged between 132 and 164 m across the entire transect, with mean elevation of 144 m in the undisturbed portion of the transect and 152 m in the disturbed portion. Disturbance within individual plots ranged from no disturbance-induced tree mortality to near complete tree mortality. Diameter at breast height (DBH, 1.3 m) was measured on all live and dead individuals greater than 10 cm

[10] https://lpdaac.usgs.gov/dataset_discovery/aster/aster_products_table/ast14dem

[11] www.vipertools.org

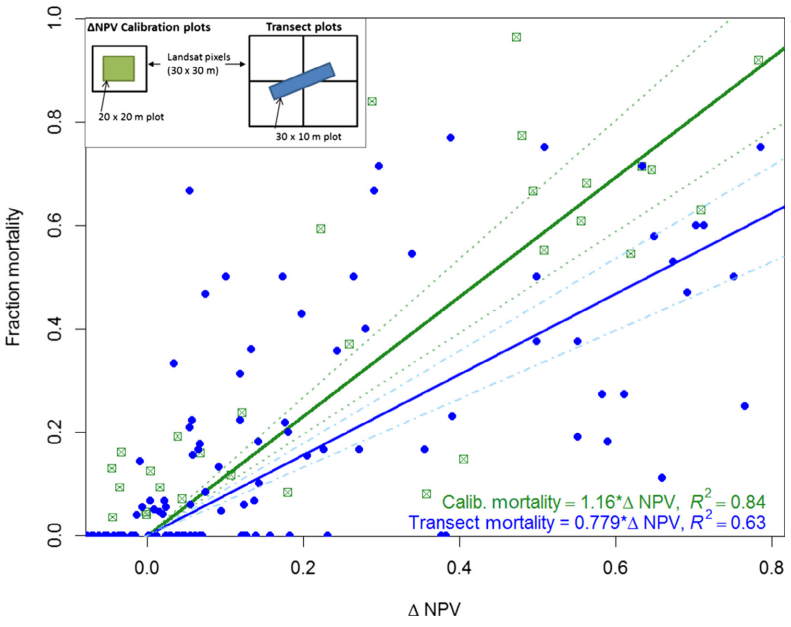


FIG. 2. The fraction of observed adult tree mortality vs. the change in pre- and post-disturbance non-photosynthetic disturbance (ΔNPV) with regressions through the origin (Model 1). The dotted and dashed lines represent the 95% credible interval for the calibration plots (green squares) and transect plots (solid blue circles). Calibration plots were carefully located to be centered on the Landsat pixels, while transect plots crossed multiple pixels.

DBH. Diameters of some dead, fallen trees were measured above 1.3 m from the base (breast height) because their boles were made inaccessible by other windthrown trees.

Approximately 95% of live trees were identified to species, and no attempt was made to identify dead trees. Dominant families in the transect plot were Lecythidaceae, Euphorbiaceae, Sapotaceae, Myristicaceae, and Fabaceae (Appendix S1: Table S4). Wood density was sampled for one live individual of each species using a gas powered drill (Tanaka TED-270PFR) by collecting all wood chips produced by drilling into the tree from the cambium to the pith with an 18 mm wide ship auger bit. The hole's volume produced by drilling was measured with vernier calipers, and the mass of the oven dried wood shavings was divided by the hole volume to determine wood density (Francis 1994). These wood density values were compared with matching species (when available) that had replicated values from the Global Wood Density Database (Chave et al. 2009, Zanne et al. 2009) to ensure the method was comparable to previously published measurements (Appendix S1: Fig. S11). Wood density samples were also collected via chainsaw for all dead individuals. Dead wood samples were submerged for 3 d to approximate their pre-death green volume, after which the volume was determined using the water balance submersion method. Samples were then oven-dried and weighed.

A separate but closely located set of 30 20 × 20 m plots (hereafter referred to as the "ΔNPV calibration plots") was installed in the same blowdown to calibrate the remote sensing-derived disturbance intensity metric (ΔNPV) to tree mortality. Unlike the transect plots, each calibration plot was installed so its center would be as close as possible to the corresponding post-disturbance Landsat 5 TM pixel (Fig. 2, inset). Each tree greater than 10 cm DBH with its base in the plot was counted and categorized as live or dead. Because our aim was to quantify blowdown mortality, we only counted dead trees that were snapped or windthrown. Snapped but resprouted trees, as well as live trees that were partially uprooted, were counted as being alive despite being likely to die within a few years. Thus, the ΔNPV metric in this study only describes immediate post-disturbance mortality and does not incorporate delayed tree mortality resulting from the disturbance.

### *Modeling tree mortality rates*

*Overview of mortality models.*—We briefly introduce four different models used to quantify how both differential mortality from the blowdown event and spatial autocorrelation affect estimates of landscape necromass produced by the blowdown. Details of each model are presented in the subsequent sections. Model 1 predicted the overall fraction of tree mortality within a pixel by regressing the overall fraction of tree mortality solely against the pixel's ΔNPV (Chambers et al. 2007). Model 2 predicted individual tree-level probability of death from the blowdown event by fitting a logistic regression of mortality probability as a function of tree size and wood density within each of six categories of disturbance intensity (ΔNPV). Model

3 was similar to Model 2, but treated ΔNPV as a continuous variable in addition to topographic position, tree size, and wood density. Model 4 was similar to Model 3, but also accounted for spatial autocorrelation. Model 1 was fit twice, once using the transect data (also used to fit Models 2–4), but also fit with the ΔNPV calibration plot data to generate an estimate of the ΔNPV–mortality relationship with reduced uncertainty in the ΔNPV predictor (see Fig. 2, inset). Models 1–4 were fit to the transect data in a Bayesian modeling framework using either Markov chain Monte Carlo (MCMC; for Models 1–3) or nested Laplace approximation (for Model 4) to estimate the model parameters. The joint posterior distribution of parameters for each model was then used to simulate the landscape necromass produced by the blowdown while propagating model uncertainty.

*Model 1: Pixel-scale mortality depends on ΔNPV.*—Following Chambers et al. (2007), tree mortality from the blowdown was estimated from ΔNPV for each pixel using a simple linear regression,

$$\%\,\text{mortality} = \beta \times \Delta\text{NPV} + \epsilon. \quad (1)$$

No intercept term was used to ensure that the predicted tree mortality was zero when ΔNPV = 0, as we were only trying to capture mortality related to disturbance (and thus ΔNPV) rather than background mortality. Forcing the relationship through the origin was also necessary to reduce bias in the lower portion of the ΔNPV and to constrain the over-prediction of necromass (see *Methods: Landscape simulation of blowdown necromass*). For purposes of comparison of the relationship with an intercept, the model fit with intercept is included in Appendix S1: Fig. S12. As explained previously, the model was fit separately to each of two different datasets: the transect data and the ΔNPV calibration plots. Each ΔNPV calibration plot was spatially located at the center of a Landsat pixel, whereas the transect plots intercepted one to four Landsat pixels (Fig. 2, inset). The lack of a one-to-one correspondence between a transect plot and a Landsat pixel is expected to increase uncertainty in the explanatory variable (ΔNPV); we explore the implications of this uncertainty in *Discussion: Differential tree mortality resulting from catastrophic wind disturbance*. The posterior distribution of the slope and standard deviation were obtained using MCMC methods implemented in the R package FilzbachR (Lyutsarev and Purves 2013).

*Model 2: Individual-tree mortality depends on tree size and wood density within ΔNPV classes.*—Model 2 assumed that the probability of mortality ($P_M$) for an individual tree depended on tree size (DBH) and wood density (WD) as,

$$P_M = \frac{1}{1 + e^{-(\beta_0 + \beta_1 \times \text{DBH} + \beta_2 \times \text{WD})}}, \quad (2)$$

where $\beta_0$ is the intercept term. The model was fit as a generalized linear mixed model (GLMM) with intercept and slope parameters treated as random effects that varied across six groups of transect plots partitioned by ΔNPV class (<0, 0–0.04, 0.041–0.15, 0.151–0.4, 0.41–0.7, and >0.71, with higher values indicating greater disturbance severity). The ranges of the ΔNPV groups were set to more evenly distribute observations of live and dead trees. Including elevation did not improve fit in Model 2, likely because elevation was correlated with ΔNPV ($r = 0.468$; Appendix S1: Fig. S10). The GLMM was fit using the Gibbs sampling MCMC package, JAGS (version 3.4.0) in conjunction with the R package, rjags (Plummer 2014).

*Model 3: Individual-tree mortality depends on ΔNPV, elevation, tree size, and wood density.*—Model 3 assumed that the probability of mortality ($P_M$) for an individual tree depended on DBH and WD, as well as a transect plot's ΔNPV and topographic position (elevation), according to a logistic function generalized linear model (GLM),

$$P_m = \frac{1}{1 + e^{-(\beta_0 + \beta_1 \times \Delta\text{NPV} + \beta_2 \times \text{DBH} + \beta_3 \times \text{WD} + \beta_4 \times \text{ELEV} + \beta_5 \times \Delta\text{NPV} \times \text{DBH} + \beta_6 \times \Delta\text{NPV} \times \text{WD})}}, \quad (3)$$

where $\beta_0$ is the intercept, and ELEV is elevation. Eq. 3 was fit using the R package FilzbachR. Model selection (i.e., inclusion/exclusion of certain interaction terms) is explained in *Methods: Model selection and assessment*.

*Model 4: Individual-tree mortality with spatial dependence.*—As explained in the introduction, tree mortality within a blowdown is an inherently spatial process, because the survival of an individual tree partially depends on whether its neighbors have been killed. To account for this spatial dependence, we used the stochastic partial differential equation GLM in the INLA package for R (Rue et al. 2009, Lindgren et al. 2011, Beguin et al. 2012). In this model (hereafter "spatial GLM"), a spatial random effect (SRE; constrained to have a mean of 0) is used to model a continuous random spatial process. The SRE term is as an additive model term (for each spatial location) that accounts for spatial dependence between observations, with the value of the SRE term varying among the spatial locations in a spatially autocorrelated manner (Beguin et al. 2012). The degree and scale of autocorrelation is not prescribed but rather is determined by the structure of the data as part of the model fitting procedure. Model 4 has the same form as

Model 3, but with the SRE term included to account for spatially autocorrelated variation in mortality,

$$P_m = \frac{1}{1 + e^{-(\beta_0+\beta_1\times\Delta NPV+\beta_2\times DBH+\beta_3\times WD+\beta_4\times ELEV+\beta_5\times\Delta NPV\times DBH+\beta_6\times\Delta NPV\times WD+SRE)}}. \quad (4)$$

In addition to sharing a common form with Model 3, this model form was confirmed by a formal selection procedure.

### *Model selection and assessment*

For the first three models, the selection of covariate combinations was guided by Akaike's information criteria, whereas the deviance information criteria (Spiegelhalter et al. 2002) was used for the spatial GLM. To compare the performance of the different models, we calculated two goodness-of-fit indices for each model: the ratio of predicted to observed necromass in the transect plots and the coefficient of determination ($R^2$) where $R^2 = 1 - (\text{sum of squares}_{\text{Residual}})/(\text{sum of squares}_{\text{Total}})$. $R^2$ was calculated for individual trees and individual transect plots. The pixel ΔNPV of 27% of the landscape encompassing the blowdown, and 15.5% of the transect subplots were <0 (Appendix S1: Fig. S8). Negative ΔNPV occurs when pixels in the post-disturbance image exhibit less NPV than the corresponding pixels in the pre-disturbance image. The linear pixel-scale ΔNPV model (Model 1) predicts negative necromass when ΔNPV is negative. Therefore, for purposes of comparison across all models, only trees in pixels with positive ΔNPV were used to calculate $R^2$ for individual trees or by plot. Spatial autocorrelation in individual tree model residuals (which would indicate a model's failure to capture spatial dependence patterns in mortality) was assessed with Moran's *I* using the correlog function in the pgirmess R package (Giraudoux 2014). Residuals were considered to be spatially autocorrelated if Moran's *I* was significantly different from zero ($P < 0.05$).

### *Landscape simulation of blowdown necromass*

We used results from the four statistical models with a simple simulation model to compare the estimated total landscape-scale necromass generated by the blowdown. For each model, we combined the estimated parameters (and uncertainties) with ΔNPV and ASTER DEM values to simulate necromass in 30 × 30 m pixels across a 500.5-ha area (5,561 pixels) that includes the blowdown. In each pixel, we simulated the mortality (or survivorship) of 50 trees, which was the mean number of trees present in a pixel area as estimated from the non-disturbed transect plots (ΔNPV < 0). The DBH and WD of the 50 trees per pixel were chosen at random from trees inventoried in the non-disturbed transect plots. The aboveground biomass of each tree was estimated from its DBH and wood density using an allometric equation (Eq. 2.1 from Chave et al. 2005). For Model 1, the estimated mortality fraction of each pixel was drawn from a normal distribution with a mean of the pixel ΔNPV multiplied by the slope β, with standard deviation σ, being drawn from the posterior distribution of the model fit. For Models 2–4, the posterior distributions from the model fits were used to parameterize the probability of death functions (Eqs. 2–4) for each individual tree in the simulated landscape. The spatial GLM (Model 4) indicated that the spatial random effect increased with disturbance intensity (Appendix S1: Fig. S2), so the simulation required predictions of SRE across the landscape, which were obtained by fitting the SRE as a third degree polynomial predicted from the ΔNPV (see Appendix S1: Fig. S2 for details). To propagate model uncertainty, 1,000 sets of parameter values were drawn from each model's joint posterior distribution and used for each of 1,000 simulations to generate a distribution of landscape necromass predictions for each model. For Model 4, each of the 1,000 parameter sets included a random draw from the sampling distribution of the polynomial SRE model fit to ΔNPV (Appendix S1: Fig. S2).

## Results

### *Overview*

The probability of individual tree mortality in the blowdown increased with both tree size and elevation, while it decreased with wood density (Fig. 3). The choice of model as assessed by goodness of fit had a large impact on simulated landscape necromass. The linear ΔNPV model (Model 1), which did not include differential tree mortality, most underpredicted the amount of necromass in the transect data (Table 2), while the spatial GLM (Model 4), which included differential tree mortality and accounted for spatial autocorrelation in mortality, most closely predicted the observed necromass in the transect data.

### *Plot-based tree mortality estimates*

The plot-based model predicting the fraction of mortality linearly from ΔNPV using the transect inventory data (Model 1) yielded a slope of 0.776 with $\epsilon \sim N(\mu = 0.04, \sigma^2 = 0.032)$ and $R^2 = 0.632$. When fit with the calibration plots, the slope was estimated to be 1.156 with $\epsilon \sim N(\mu = 0.05, \sigma^2 = 0.039)$ and $R^2 = 0.845$ (Fig. 2). Both ΔNPV slope estimates are similar to prior studies (slope of 0.996 in Chambers et al. 2007, 1.03 in Negrón-Juárez et al. 2010).

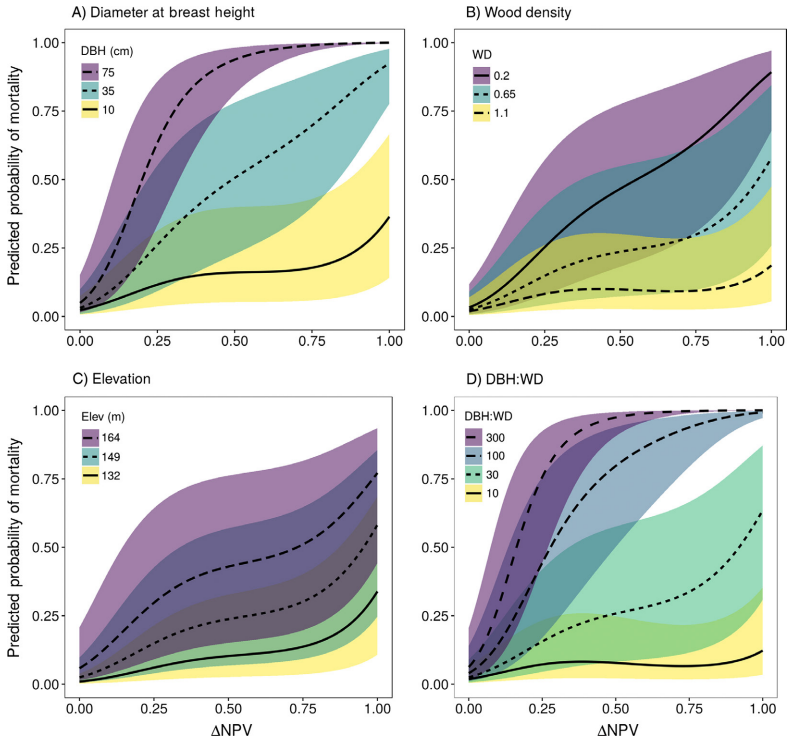


FIG. 3. Estimated probability of mortality from a catastrophic wind disturbance of a tree with median tree characteristics, as predicted by the spatial logistic regression model with the SRE (Model 4). Shaded regions represent 95% confidence interval as calculated by the Delta Method (Jackson 2011). The median tree characteristics were 17.3 cm DBH, 0.64 wood density, and 149 m elevation.

### *Differential tree mortality models*

Models 2–4 all indicated that tree mortality was non-random, with large trees, low wood density trees, and trees at higher elevations being the most likely to die (Fig. 3). When probability of mortality was determined with the spatial model, the largest tree in the field data (98.7 cm) was predicted to be up to five times more likely to have died than the trees with minimum diameter measured in this study (10 cm DBH) at high ΔNPV (Fig. 4). Trees with the lowest wood density (~0.18 g/cm$^3$) were up to four times more likely to die than trees with the highest wood density (~1.1 g/cm$^3$) at high levels of disturbance intensity. Model 2, the ΔNPV-partitioned GLMM, generally showed the effect size of DBH to increase with higher levels ΔNPV (Appendix S1: Table S2). The interaction between DBH and ΔNPV shows that large diameter trees are even more likely to die when disturbance intensity is high (Table 1, Figs. 3A and 4A). The interaction between WD and ΔNPV suggests that the effect of wood density towards promoting survival is stronger as disturbance intensity increases (Table 1, Figs. 3B and 4B; Appendix S1: Figs. S4 and S6). Large trees with low wood density (i.e., high DBH:WD ratio) are the most prone to die, even in the lower quarter of the ΔNPV spectrum (Fig. 3D).

### *Spatial vs. non-spatial GLM*

The spatial GLM was the only model of those tested that reduced spatial autocorrelation, as measured by Moran's *I*, to a non-significant ($P > 0.05$) level across all tested distance classes (30–1,450 m; Appendix S1: Fig. S1). The coefficient estimates for the covariates in the spatial GLM and the non-spatial version were similar (Table 1), but 95% credible intervals were narrower for the non-spatial GLM, as expected when spatial autocorrelation is ignored (Lichstein et al. 2002). The probability of mortality of individual trees was generally overpredicted by the non-spatial individual tree-based models (Models 2 and 3; Table 2; Appendix S1: Fig. S9).

### *Goodness of fit of model necromass predictions*

When comparing cumulative predicted necromass from the different models, the linear ΔNPV model (Model 1) most underpredicted the necromass (59.3% predicted:observed), while the non-spatial GLM (Model 3) most over predicted necromass (111.2%; Table 2). The spatial GLM (Model 4) predicted 91.2% of the observed necromass, and the ΔNPV-partitioned GLMM (Model 2) predicted 111.1% (Table 2). The linear ΔNPV model (Model 1) performed best at predicting necromass when $R^2$ was calculated by individual tree, while the Spatial

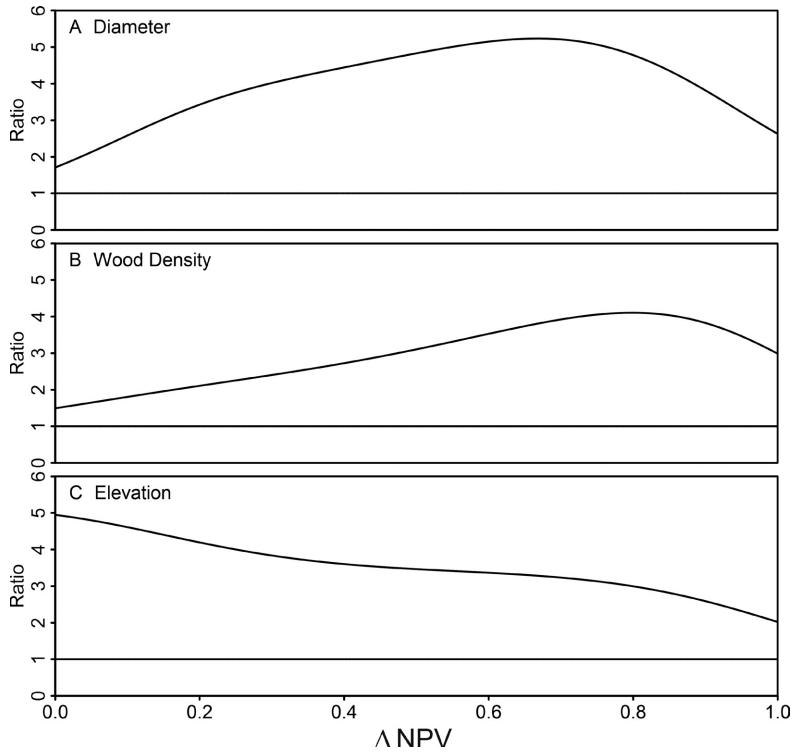


FIG. 4. The ratio of estimated mortality probabilities between small and large (2.5 and 97.5% quantiles of the transect data, respectively) for (A) tree diameter, (B) wood density, and (C) elevation as a function of disturbance intensity, illustrating the interaction between disturbance intensity and tree/site characteristics. Large and small values were: 55 and 10.3 cm DBH; 0.97 and 0.33 wood density; and 162 and 134 m elevation. The model used was the spatial GLM (Model 4). The dashed line indicates no difference in the mortality probability.

TABLE 1. β coefficients for fixed effects in a non-spatial generalized linear model (GLM; Model 3) and a spatial GLM (Model 4).

| | Non-spatial GLM | | | Spatial GLM | | |
|---|---|---|---|---|---|---|
| Effect | 2.5% | 50.0% | 97.5% | 2.5% | 50.0% | 97.5% |
| Intercept | −15.784 | −12.907 | −9.626 | −20.503 | −11.617 | −2.762 |
| ΔNPV | 0.882 | 3.404 | 6.029 | −1.564 | 2.021 | 5.648 |
| DBH | −0.006 | 0.010 | 0.025 | −0.007 | 0.012 | 0.031 |
| WD | −1.597 | −0.446 | 0.789 | −2.097 | −0.633 | 0.824 |
| Elevation | 0.050 | 0.071 | 0.091 | −0.001 | 0.059 | 0.118 |
| ΔNPV:DBH | 0.067 | 0.123 | 0.183 | 0.050 | 0.110 | 0.176 |
| ΔNPV:WD | −7.931 | −4.272 | −0.688 | −7.494 | −3.401 | 0.595 |

*Notes:* 2.5, 50, and 97.5% Bayesian credible intervals are presented. Abbreviations are ΔNPV, difference in non-photosynthetic vegetation before and after disturbance event; DBH, diameter at breast height (cm); WD, wood density (g oven dry/cm$^3$ green volume); Elevation (m); ΔNPV:DBH, ΔNPV interaction with diameter; ΔNPV:WD, ΔNPV interaction with wood density.

GLM (Model 4) performed best when $R^2$ was calculated by plot (Table 2).

### *Landscape necromass estimation from simulation modeling*

The linear ΔNPV model (Model 1) that used the transect data rather than the calibration data predicted the least necromass across the landscape (Fig. 5). Compared to this model, the ΔNPV-partitioned GLMM (Model 2), the spatial GLM (Model 4), and the non-spatial GLM (Model 3) models predicted 67.9%, 51%, and 93.6% more necromass, respectively (Appendix S1: Table S3). The linear ΔNPV model (Model 1) parameterized from the ΔNPV calibration plots predicted 31.5% more landscape-level necromass than the same model parameterized from the transect data. The uncertainty of cumulative landscape necromass estimates

TABLE 2. Goodness of fit between model necromass predictions and observed necromass from transect plot data.

| Model | General description | Spatial | Traits | Question | $R^2_{tree}$ | $R^2_{plot}$ | $\frac{\text{Pred.}}{\text{Obs.}}$ |
|---|---|---|---|---|---|---|---|
| Linear ΔNPV- calibration data (1) | Predicts fraction of adult tree mortality from blowdown; fit with ΔNPV calibration plot data. | no | no | baseline | 0.45 | 0.57 | 0.88 |
| Linear ΔNPV- transect data (1) | Predicts fraction of adult tree mortality from blowdown; fit with transect plot data. | no | no | baseline | 0.38 | 0.47 | 0.59 |
| ΔNPV partitioned GLMM (2) | Hierarchical model that predicts individual mortality using DBH and WD; partitioned by disturbance intensity using ΔNPV (binned). | no | yes | Q1 | 0.21 | 0.54 | 1.11 |
| Non-spatial GLM (3) | Predicts individual mortality using ΔNPV (continuous), DBH, WD, and elevation. | no | yes | Q1 | 0.29 | 0.55 | 1.11 |
| Spatial GLM (4) | Same as non-spatial GLM, but accounts for spatial dependence between observations. | yes | yes | Q2 & Q3 | 0.34 | 0.58 | 0.91 |

*Notes:* The model number is listed in parentheses. Traits included diameter at breast height (DBH) and wood density (WD). Q1–3 are reference questions from last paragraph of introduction.

varied considerably among the different models (Fig. 5; Appendix S1: Table S3). The ΔNPV-partitioned GLMM (Model 2) and the spatial GLM allocated considerably less necromass into pixels with negative ΔNPV than the other models (Appendix S1: Table S1).

## DISCUSSION

### *Differential tree mortality resulting from catastrophic wind disturbance*

We found that tree structural attributes that enhance survival during catastrophic wind disturbance in the Peruvian Amazon are different than attributes commonly cited to promote survival during periods of background mortality. For example, large Neotropical canopy emergent trees have been observed to exhibit approximately half the annual mortality of the landscape average (Thomas et al. 2013), while other observations have suggested increasing diameter to be an inconsistent predictor of death under background mortality conditions (Chao et al. 2008). In contrast, we observed drastically higher probabilities of mortality for large trees from a catastrophic wind disturbance event. This contrast in predictive mortality of a trait highlights the importance of differentiating periods of background mortality from episodes of catastrophic mortality. Similarly, increased mortality has been reported for large trees near edges from fragmented forests in the central Amazon (Laurance et al. 2000), where increased exposure to wind has been suggested to be one of the root causes. This contrast in size effects between background and episodic mortality is not unique to wind disturbance, as a recent study also found a size mediated increase in mortality rates for large trees exposed to drought (Bennett et al. 2015). Forest simulators and ecosystem models may produce more accurate mortality predictions if different trait-based mortality algorithms are implemented to decide which trees die under background mortality vs. during a catastrophic disturbance event. As in Neotropical forests, blowdowns are also well documented in northern temperate forests (Canham and Loucks 1984), where the size dependent effect upon tree mortality has also been observed from storm windthrow events in the Adirondack mountains of New York, USA (Canham et al. 2001), a 236,000-ha blowdown in the southern boreal forests of Minnesota, USA (Rich et al. 2007), and in tree mortality from tornado impacted forests in the Eastern USA (Peterson 2007). In our study, the probability of small tree mortality only increased at very high values of ΔNPV (Fig. 3A), which suggests that wind disturbance only affects small trees if disturbance is severe enough to kill many large trees. This has also been observed in the central Amazon during periods of elevated wind disturbance (Toledo et al. 2012), as well as in other studies covering periods of background levels of mortality (Clark and Clark 1991, Chao et al. 2009).

Wood density has often been cited as a predictor of background tree mortality in tropical forests (Chao et al. 2008), explaining ~31% of the interspecific variation in tree mortality rates across a network of large forest inventory plots (Kraft et al. 2010). Unlike tree size, wood density likely promotes survival through both periods of background and catastrophic mortality as wood density is highly correlated with strength (Niklas 1992), which is important because branch-fall is a major source of damage for understory and sub-canopy trees (Clark and Clark 1991). Tree diameter, wood density, elevation, and disturbance intensity interacted to alter the probability of mortality within a blowdown. For example, the

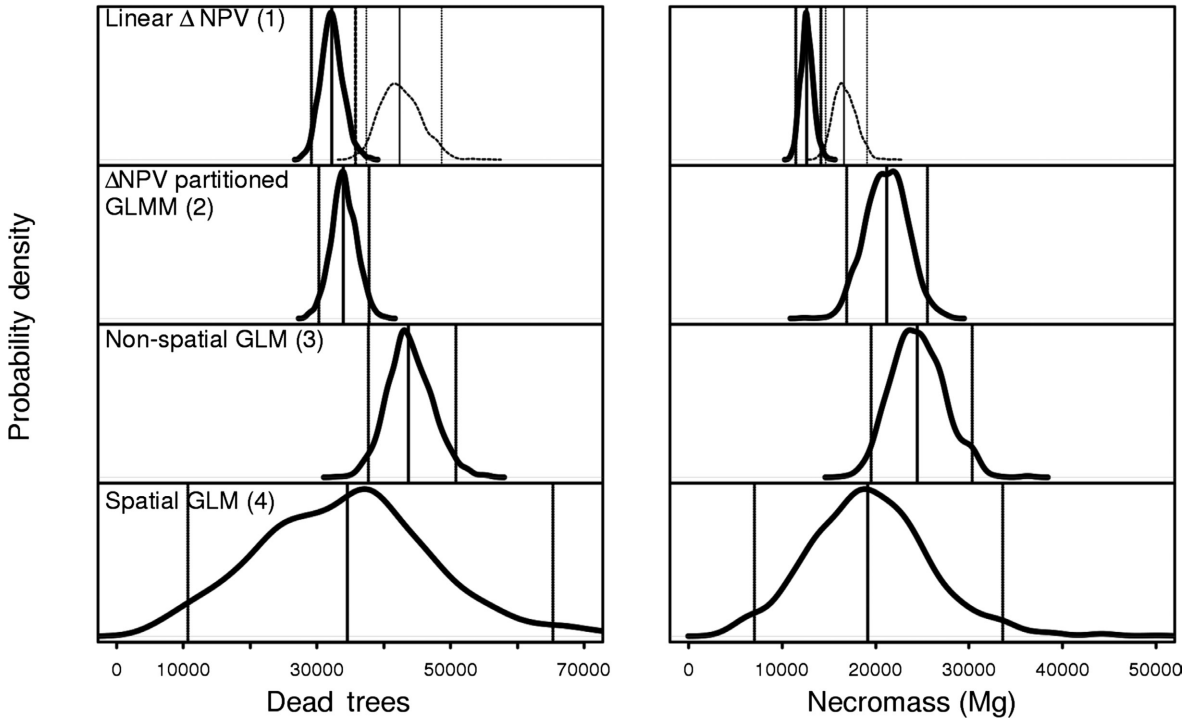


Fig. 5. Total estimated tree mortality (left column) and corresponding necromass (right column) from the simulated landscape using four different models. For Model 1, the dark line represents the simulation from the model fit from the transect data and the dotted line represents the simulation generated from the model fit with the calibration data. For all other models, only the transect data was used. Solid vertical lines represent the 50% quantile, while dotted lines represent the 2.5 and 97.5%.

difference in probability of death between low and high wood density trees is not as large as differences in mortality due to size or elevation (Figs. 3 and 4), yet when wood density is coupled with tree size, the differences in probability of death are at their most extreme (Fig. 3D; Appendix S1: Fig. S5), in that large trees with low wood density are especially likely to die in a wind disturbance.

For this blowdown, individual trees at higher elevation were more prone to die (Table 1, Figs. 3 and 4). The blowdown epicenter was located on a ridge, so this elevation effect on mortality may not be translatable to wind disturbances with epicenters on floodplains or depressions. Yet in a study from the central Amazon, approximately one quarter of the variation in tree mortality across a time interval with multiple wind storms could be attributed to variation in topography and soil fertility (Toledo et al. 2011). Potentially this could be due to increased exposure to high wind speeds on ridges that remove large individuals (Everham and Brokaw 1996), enhanced drought stress on ridges (Silva et al. 2013), or some combination of the two factors.

At very high levels of disturbance intensity, individual differences in diameter and elevation position become less important in differentiating which trees will die (Fig. 4). This may be explained by two interrelated causes: (1) as disturbance intensity increases and the fraction of trees that die approaches 1, mortality (by definition) becomes less discriminating, and (2) as disturbance intensity increases, each tree is under greater risk of being crushed or damaged by a neighboring tree. We cite two results to support the second claim. First, the SRE term of the spatial GLM, which captures the influence of neighboring trees on an individual's probability of mortality, increased the probability of mortality when $\Delta NPV > 0.065$ and plateaued when $\Delta NPV > 0.3$ (Appendix S1: Fig. S2). Second, we found the difference in probability of mortality between high and low WD trees increased with ΔNPV (Fig. 4), which is consistent with the idea that high WD should promote survival from damage caused by falling neighbors.

Our estimated landscape necromass is most likely an underestimate of the actual longer-term necromass produced by the blowdown because only the number of trees killed within one year of the blowdown is estimated, while more died in the years following. Second, linear modeling of the ΔNPV metric is not robust to detecting treefall events composed of fewer than six trees (Negrón-Juárez et al. 2011), so many smaller treefall events were undetected. Finally, coarse woody debris that results from mechanisms other than tree mortality, including crown breakage and branchfall, likely represent a significant contribution to the true necromass pool created in the blowdown. For example, Palace et al. (2008) found

that coarse necromass was underestimated by 45% when only derived from tree mortality rates.

### *Implications of spatial autocorrelation for estimating mortality effects and landscape-scale necromass*

Landscape necromass simulations using the spatial GLM predicted 51% more necromass than the linear ΔNPV model with random-mortality fit using the transect data, yet only 15% more necromass than the random mortality linear ΔNPV fit using the calibration data. The difference in necromass estimates was a direct result of the difference in the slope parameters between the linear regression models, where the slope of the transect fit (0.78) was lower than the calibration plot fit (1.16). This discrepancy was likely the result of the rectangular transect plots spanning multiple ΔNPV pixels (thereby introducing error in the explanatory variable and reducing its effect size; Lichstein et al. 2014), whereas the square calibration plots were located within the center of a single pixel. The ΔNPV error induced by crossing multiple pixels in the transect data is likely what caused the reduced slope in the ΔNPV–mortality relationship fit with the transect data (Fig. 2.). It is likely this misalignment also served to reduce the effect size of the ΔNPV term in the differential mortality models and reduced their overall ability to explain variation in mortality between individuals.

The clarity of the linear mortality–ΔNPV relationship was also obscured by the study region's occasional complex topography. Slopes in excess of 45° (30-m scale) are not uncommon in the study region, producing a complex pattern of illumination and shading on top of the canopy, which in turn affects ΔNPV estimates. Two of the three largest model residuals in the relationship from the ΔNPV calibration plots were from areas where the field measured sub-plot slope was in excess of 35°. Despite the complex topography, the estimated slopes of the linear mortality–ΔNPV relationships are fairly consistent with what has been estimated from studies in other tropical forest landscapes (Negrón-Juárez et al. 2010, 2011).

Whereas the overall heterogeneity of disturbed forest patches across the blowdown was captured by mapping ΔNPV, addressing spatial dependence between pixels and between individual tree-level observations was crucial to constraining the predictions for a tree's probability of death. The coefficients for DBH, wood density and elevation in the non-spatial and spatial GLMs were generally similar (Table 1), yet the inclusion of the spatial random effect in the spatial GLM better constrained the estimation of necromass in the lower range of the ΔNPV spectrum. For example, the simulated average necromass per killed tree was similar between both the non-spatial and the spatial GLMs (Appendix S1: Fig. S7), yet the non-spatial GLM simulation of landscape disturbance estimated 26% more tree death and >27% more necromass than the spatial GLM. This discrepancy was due to the non-spatial GLM estimating more necromass in the lower ΔNPV range of pixels (Appendix S1: Table S1 and Fig. S9), whereas the SRE of the spatial GLM increased survival when ΔNPV was under 0.065, and increased mortality when ΔNPV was higher (Appendix S1: Figs. S2 and S3).

It was essential that in scaling up necromass predictions from the plot to the landscape level that mortality was not overpredicted in the lower portion of the disturbance intensity spectrum because the majority of pixels in the landscape encompassing the blowdown have low ΔNPV values (Appendix S1: Fig. S8). Because the spatial GLM model's residuals were not spatially autocorrelated, had the smallest error of predicted:observed necromass, did not overpredict mortality in the low ΔNPV pixels, and produced the highest $R^2$ for predicted necromass by individual plot, we suggest that the spatial GLM provides the best model to estimate landscape necromass.

## Conclusions

We found that two factors, differential mortality and the spatial structure of mortality, acted independently to affect total necromass on the landscape. Simple relationships relating tree mortality to disturbance metrics in tropical forests can oversimplify the complex processes that create important variation in tree mortality related to tree and landscape characteristics. We show evidence of differential mortality within a northwestern Amazon forest affected by a catastrophic wind disturbance event. While estimating landscape necromass with the linear ΔNPV relationship coupled with random mortality is by far the easiest to implement, we conservatively estimate that this method underpredicts total blowdown necromass by 15–51% for the blowdown documented here. Probabilistic estimation of tree mortality is better approached when underlying spatial processes are included in models of tree mortality. Failure to account for spatial autocorrelation may produce undue confidence in parameter estimates, of which even small differences can result in large estimation discrepancies when scaled to the landscape. Whereas tree death from wind disturbance and differential probability of death have sometimes been incorporated into local scale gap dynamic models, this has yet to be incorporated into larger regional scale forest carbon models. Incorporating differential mortality from wind disturbance is likely to augment estimates of forest biomass lost because of the strong predisposition of large trees to die.

## Acknowledgments

Conducted research was funded by the NASA Biodiversity Program (Project NNX09AK21G). S. W. Rifai was supported by a NASA Earth and Space Science Graduate Fellowship. R. Negrón-Juárez was supported by Next-Generation Ecosystems Experiments-Tropics (NGEE Tropics) and the Regional and Global Climate Modeling (RGCM) program funded by the U.S. Department of Energy, Office of Science, Office of Biological and Environmental Research. We greatly acknowledge the

field assistance of Jarli Isuiza, Pablo Marin Ruiz, and Randal Regnifo. We also thank two anonymous reviewers for comments that improved the manuscript.

## Literature Cited

Asner, G. P. 2013. Geography of forest disturbance. Proceedings of the National Academy of Sciences USA 110:3711–3712.

Barlow, J., C. A. Peres, B. O. Lagan, and T. Haugaasen. 2003. Large tree mortality and the decline of forest biomass following Amazonian wildfires. Ecology Letters 6:6–8.

Beguin, J., S. Martino, H. Rue, and S. G. Cumming. 2012. Hierarchical analysis of spatially autocorrelated ecological data using integrated nested Laplace approximation. Methods in Ecology and Evolution 3:921–929.

Bennett, A. C., N. G. McDowell, C. D. Allen, and K. J. Anderson-Teixeira. 2015. Larger trees suffer most during drought in forests worldwide. Nature Plants 1:15139.

Brokaw, N. V. L., and J. S. Grear. 1991. Forest structure before and after hurricane hugo at three elevations in the Luquillo mountains, Puerto Rico. Biotropica 23:386.

Canham, C. D., and O. L. Loucks. 1984. Catastrophic windthrow in the presettlement forests of Wisconsin. Ecology 65:803.

Canham, C. D., M. J. Papaik, and E. F. Latty. 2001. Interspecific variation in susceptibility to windthrow as a function of tree size and storm severity for northern temperate tree species. Canadian Journal of Forest Research-Revue Canadienne De Recherche Forestiere 31:1–10.

Chambers, J. Q., J. I. Fisher, H. Zeng, E. L. Chapman, D. B. Baker, and G. C. Hurtt. 2007. Hurricane Katrina's carbon footprint on U.S. Gulf coast forests. Science 318:1107.

Chambers, J. Q., R. I. Negrón-Juárez, G. C. Hurtt, D. M. Marra, and N. Higuchi. 2009a. Lack of intermediate-scale disturbance data prevents robust extrapolation of plot-level tree mortality rates for old-growth tropical forests. Ecology Letters 12:E22–E25.

Chambers, J. Q., A. L. Robertson, V. M. C. Carneiro, A. J. N. Lima, M.-L. Smith, L. C. Plourde, and N. Higuchi. 2009b. Hyperspectral remote detection of niche partitioning among canopy trees driven by blowdown gap disturbances in the Central Amazon. Oecologia 160:107–117.

Chambers, J. Q., R. I. Negrón-Juárez, D. M. Marra, A. D. Vittorio, J. Tews, D. Roberts, G. H. P. M. Ribeiro, S. E. Trumbore, and N. Higuchi. 2013. The steady-state mosaic of disturbance and succession across an old-growth Central Amazon forest landscape. Proceedings of the National Academy of Sciences USA 110:3949–3954.

Chao, K.-J., O. L. Phillips, E. Gloor, A. Monteagudo, A. Torres-Lezama, and R. V. Martínez. 2008. Growth and wood density predict tree mortality in Amazon forests. Journal of Ecology 96:281–292.

Chao, K.-J., O. L. Phillips, A. Monteagudo, A. Torres-Lezama, and R. Vásquez Martínez. 2009. How do trees die? Mode of death in northern Amazonia. Journal of Vegetation Science 20:260–268.

Chave, J., et al. 2005. Tree allometry and improved estimation of carbon stocks and balance in tropical forests. Oecologia 145:87–99.

Chave, J., D. Coomes, S. Jansen, S. L. Lewis, N. G. Swenson, and A. E. Zanne. 2009. Towards a worldwide wood economics spectrum. Ecology Letters 12:351–366.

Clark, D. B., and D. A. Clark. 1991. The impact of physical damage on canopy tree regeneration in tropical rain forest. Journal of Ecology 79:447–457.

Clark, D. B., and D. A. Clark. 1996. Abundance, growth and mortality of very large trees in neotropical lowland rain forest. Forest Ecology and Management 80:235–244.

Curran, T. J., L. N. Gersbach, W. Edwards, and A. K. Krockenberger. 2008. Wood density predicts plant damage and vegetative recovery rates caused by cyclone disturbance in tropical rainforest tree species of North Queensland, Australia. Austral Ecology 33:442–450.

Davidson, E. A., et al. 2012. The Amazon basin in transition. Nature 481:321–328.

Everham, E. M., and N. V. L. Brokaw. 1996. Forest damage and recovery from catastrophic wind. Botanical Review 62:113–185.

Fisher, J., G. Hurtt, R. Thomas, and J. Chambers. 2008. Clustered disturbances lead to bias in large-scale estimates based on forest sample plots. Ecology Letters 11:554–563.

Francis, J. K. 1994. Simple and inexpensive method for extracting wood density samples from tropical hardwoods. Tree Planters' Notes 45:10–12.

Garstang, M., S. White, H. H. Shugart, and J. Halverson. 1998. Convective cloud downdrafts as the cause of large blowdowns in the Amazon rainforest. Meteorology and Atmospheric Physics 67:199–212.

Giraudoux, P. 2014. pgirmess: Data analysis in ecology.

Jackson, C. 2011. Multi-state models for panel data: the msm package for R. Journal of Statistical Software 38(8):1–29.

Kellner, J. R., and G. P. Asner. 2009. Convergent structural responses of tropical forests to diverse disturbance regimes. Ecology Letters 12:887–897.

Kraft, N. J. B., M. R. Metz, R. S. Condit, and J. Chave. 2010. The relationship between wood density and mortality in a global tropical forest data set. New Phytologist 188:1124–1136.

Laurance, W. F., P. Delamônica, S. G. Laurance, H. L. Vasconcelos, and T. E. Lovejoy. 2000. Conservation: rainforest fragmentation kills big trees. Nature 404:836.

Lichstein, J. W., T. R. Simons, S. A. Shriner, and K. E. Franzreb. 2002. Spatial autocorrelation and autoregressive models in ecology. Ecological Monographs 72:445–463.

Lichstein, J. W., N.-Z. Golaz, S. Malyshev, E. Shevliakova, T. Zhang, J. Sheffield, R. A. Birdsey, J. L. Sarmiento, and S. W. Pacala. 2014. Confronting terrestrial biosphere models with forest inventory data. Ecological Applications 24:699–715.

Lindgren, F., H. Rue, and J. Lindström. 2011. An explicit link between Gaussian fields and Gaussian Markov random fields: the stochastic partial differential equation approach. Journal of the Royal Statistical Society B 73:423–498.

Lugo, A. E., and F. N. Scatena. 1996. Background and catastrophic tree mortality in tropical moist, wet, and rain forests. Biotropica 28:585–599.

Lyutsarev, V., and D. Purves. 2013. filzbach: Filzbach MCMC sampler. R package version 0.6-1. http://research.microsoft.com/en-us/um/cambridge/groups/science/tools/filzbach/filzbach.htm

Marra, D. M., J. Q. Chambers, N. Higuchi, S. E. Trumbore, G. H. P. M. Ribeiro, J. dos Santos, R. I. Negrón-Juárez, B. Reu, and C. Wirth. 2014. Large-scale wind disturbances promote tree diversity in a central Amazon forest. PLoS ONE 9:e103711.

Negrón-Juárez, R. I., J. Q. Chambers, G. Guimaraes, H. Zeng, C. F. M. Raupp, D. M. Marra, G. H. P. M. Ribeiro, S. S. Saatchi, B. W. Nelson, and N. Higuchi. 2010. Widespread Amazon forest tree mortality from a single cross-basin squall line event. Geophysical Research Letters 37:L16701, doi:10.1029/2010GL043733.

Negrón-Juárez, R. I., J. Q. Chambers, D. M. Marra, G. H. P. M. Ribeiro, S. W. Rifai, N. Higuchi, and D. Roberts. 2011. Detection of subpixel treefall gaps with Landsat imagery in Central Amazon forests. Remote Sensing of Environment 115:3322–3328.

Nelson, B. W., V. Kapos, J. B. Adams, W. J. Oliveira, and O. P. G. Braun. 1994. Forest disturbance by large blowdowns in the Brazilian Amazon. Ecology 75:853.

Nepstad, D. C., I. M. Tohver, D. Ray, P. Moutinho, and G. Cardinot. 2007. Mortality of large trees and lianas following experimental drought in an Amazon forest. Ecology 88:2259–2269.

Niklas, K. J. 1992. Plant biomechanics: an engineering approach to plant form and function. University of Chicago Press, Chicago, Illinois, USA.

Palace, M., M. Keller, and H. Silva. 2008. Necromass production: studies in undisturbed and logged Amazon forests. Ecological Applications 18:873–884.

Peterson, C. J. 2007. Consistent influence of tree diameter and species on damage in nine eastern North America tornado blowdowns. Forest Ecology and Management 250:96–108.

Plummer, M. 2014. rjags: Bayesian graphical models using MCMC. R package version 3-15. http://CRAN.R-project.org/package=rjags

Rich, R. L., L. E. Frelich, and P. B. Reich. 2007. Wind-throw mortality in the southern boreal forest: effects of species, diameter and stand age. Journal of Ecology 95:1261–1273.

Roberts, D. A., M. Gardner, R. Church, S. Ustin, G. Scheer, and R. O. Green. 1998. Mapping chaparral in the Santa Monica Mountains using multiple endmember spectral mixture models: II. Environmental influences on regional abundance. Remote Sensing of Environment 65:267–279.

Rue, H., S. Martino, and N. Chopin. 2009. Approximate Bayesian inference for latent Gaussian models by using integrated nested Laplace approximations. Journal of the Royal Statistical Society B 71:319–392.

Silva, C. E., J. R. Kellner, D. B. Clark, and D. A. Clark. 2013. Response of an old-growth tropical rainforest to transient high temperature and drought. Global Change Biology 19:3423–3434.

Sinton, D. S., J. A. Jones, J. L. Ohmann, and F. J. Swanson. 2000. Windthrow disturbance, forest composition, and structure in the Bull Run basin, Oregon. Ecology 81:2539–2556.

Sombroek, W. 2001. Spatial and temporal patterns of Amazon rainfall. AMBIO: A Journal of the Human Environment 30:388–396.

Spiegelhalter, D. J., N. G. Best, B. P. Carlin, and A. van der Linde. 2002. Bayesian measures of model complexity and fit. Journal of the Royal Statistical Society B 64:583–639.

Thomas, R. Q., J. R. Kellner, D. B. Clark, and D. R. Peart. 2013. Low mortality in tall tropical trees. Ecology 94:920–929.

Toledo, J. J., W. E. Magnusson, C. V. Castilho, and H. E. M. Nascimento. 2011. How much variation in tree mortality is predicted by soil and topography in Central Amazonia? Forest Ecology and Management 262:331–338.

Toledo, J. J., W. E. Magnusson, C. V. Castilho, and H. E. M. Nascimento. 2012. Tree mode of death in Central Amazonia: effects of soil and topography on tree mortality associated with storm disturbances. Forest Ecology and Management 263:253–261.

Zanne, A. E., G. Lopez-Gonzalez, D. A. Coomes, J. Ilic, S. Jansen, S. L. Lewis, R. B. Miller, N. G. Swenson, M. C. Wiemann, and J. Chave. 2009. Data from: towards a worldwide wood economics spectrum. Dryad Digital Repository. http://dx.doi.org/10.5061/dryad.234

## Supporting Information

Additional supporting information may be found in the online version of this article at http://onlinelibrary.wiley.com/doi/10.1002/eap.1368/suppinfo